Functional Analysis of the Cellulose Synthase-Like Genes *CSLD1*, *CSLD2*, and *CSLD4* in Tip-Growing Arabidopsis Cells[1][W]

Adriana J. Bernal[2], Cheol-Min Yoo[2], Marek Mutwil[3], Jakob Krüger Jensen, Guichuan Hou, Claudia Blaukopf, Iben Sørensen, Elison B. Blancaflor, Henrik Vibe Scheller[4], and William G.T. Willats*

Department of Biology, University of Copenhagen, Copenhagen Biocentre, 2200 Copenhagen, Denmark (A.J.B., M.M., C.B., I.S., W.G.T.W.); Plant Biology Division, Samuel Roberts Noble Foundation, Ardmore, Oklahoma 73401 (C.-M.Y., E.B.B.); Plant Biochemistry Laboratory, University of Copenhagen, DK–1871 Frederiksberg C, Denmark (J.K.J., H.V.S.); Dewel Microscopy Facility, Appalachian State University, Boone, North Carolina 28608 (G.H.); and Departamento de Ciencias Biológicas, Universidad de los Andes, Bogotá, Colombia (A.J.B.)

A reverse genetic approach was used to investigate the functions of three members of the cellulose synthase superfamily in Arabidopsis (*Arabidopsis thaliana*), *CELLULOSE SYNTHASE-LIKE D1* (*CSLD1*), *CSLD2*, and *CSLD4*. *CSLD2* is required for normal root hair growth but has a different role from that previously described for *CSLD3* (*KOJAK*). *CSLD2* is required during a later stage of hair development than *CSLD3*, and *CSLD2* mutants produce root hairs with a range of abnormalities, with many root hairs rupturing late in development. Remarkably, though, it was often the case that in *CSLD2* mutants, tip growth would resume after rupturing of root hairs. In silico, semiquantitative reverse transcription-polymerase chain reaction, and promoter-reporter construct analyses indicated that the expression of both *CSLD2* and *CSLD3* is elevated at reduced temperatures, and the phenotypes of mutants homozygous for insertions in these genes were partially rescued by reduced temperature growth. However, this was not the case for a double mutant homozygous for insertions in both *CSLD2* and *CSLD3*, suggesting that there may be partial redundancy in the functions of these genes. Mutants in *CSLD1* and *CSLD4* had a defect in male transmission, and plants heterozygous for insertions in *CSLD1* or *CSLD4* were defective in their ability to produce pollen tubes, although the number and morphology of pollen grains was normal. We propose that the CSLD family of putative glycosyltransferases synthesize a polysaccharide that has a specialized structural role in the cell walls of tip-growing cells.

Almost all plant cells are surrounded by a carbohydrate-rich cell wall (Carpita and Gibeaut, 1993; Fry, 2004). These highly complex fiber composite structures provide support and defense for the plant body and also have important roles in signaling, cell fate, and cell-to-cell adhesion (Bacic et al., 1988; O'Neill et al., 1990; Carpita and Gibeaut, 1993; Ridley et al., 2001). Plant cell walls also affect human society, and particularly health and industry, in numerous ways. They are the largest source of biomass on earth and are an important renewable resource of high-value biopolymers with numerous industrial applications, including as feedstocks for biofuels, functional food ingredients, and industrial fibers (Kim and Triplett, 2001; Willats et al., 2006; Himmel et al., 2007; Reyna-Villasmil et al., 2007). Cell walls are constructed by the coordinated activity of a large number of biosynthetic enzymes, including glycosyl transferase (GT) enzymes that catalyze the formation of glycoside bonds in cell wall glycan polymers (Reiter, 2002; Scheible and Pauly, 2004). In Arabidopsis (*Arabidopsis thaliana*), it is thought that at least 200 GTs may be involved in cell wall biosynthesis, and steady progress has been made in identifying and characterizing these enzymes (Reiter, 2002; Scheible and Pauly, 2004). In the primary walls of growing plant tissues, the three major classes of polymer are cellulose, hemicelluloses, and pectins, and these form a coextensive network in most cells (Carpita and Gibeaut, 1993; Fry, 2004; Cosgrove, 2005). Cellulose biosynthesis is performed by cellulose synthase (CESA) GTs that are grouped in complexes at the plasma membrane. Ten CESAs have been identified in

[1] This work was supported by the Danish Research Agency (grants to A.J.B., J.K.J., I.S., H.V.S., and W.G.T.W.), the National Science Foundation (grant no. DBI–0400580 to E.B.B.), and the Samuel Roberts Noble Foundation (grants to C.-M.Y. and E.B.B.).

[2] These authors contributed equally to the article.

[3] Present address: Max-Planck-Institute of Molecular Plant Physiology, AM Mühlenberg 1, D–14476 Potsdam-Golm, Germany.

[4] Present address: Joint Bioenergy Institute, 5885 Hollis Street, Emeryville, CA 94608.

* Corresponding author; e-mail willats@bio.ku.dk.

The author responsible for distribution of materials integral to the findings presented in this article in accordance with the policy described in the Instructions for Authors (www.plantphysiol.org) is: William G.T. Willats (willats@bio.ku.dk).

[W] The online version of this article contains Web-only data.

www.plantphysiol.org/cgi/doi/10.1104/pp.108.121939

Arabidopsis, and their roles in the synthesis of primary and secondary walls have been extensively characterized (Taylor et al., 2003; Paredez et al., 2006; Desprez et al., 2007; Persson et al., 2007). In contrast, only a small fraction of the at least 54 GTs involved in pectin biosynthesis have been identified so far (Ridley et al., 2001; Sterling et al., 2006). Hemicelluloses are a family of polysaccharides that typically have roles in providing structural support by cross-linking cellulose microfibrils. Unlike cellulose, which is made exclusively from Glc, hemicelluloses are structurally diverse, and most consist of linear backbone domains with short side chains (Fry, 2004). Backbone domains can consist of (1–4)-β-D-linked mannan, xylan, glucan, and, in the case of the Poales and *Equisetum* spp., (1→3)(1→4)-β-D-glucan (Fry, 2004; Sørensen et al., 2008). Recently, several GTs involved in the synthesis of the backbones of hemicelluloses were described, and all are products of genes in the *CELLULOSE SYNTHASE-LIKE* (*CSL*) family (Dhugga et al., 2004; Liepman et al., 2005; Burton et al., 2006, 2008; Cocuron et al., 2007).

CSL genes were first identified in Arabidopsis by their similarity to the *CESA* genes, and on the basis of predicted protein sequences, these *CSL* genes were grouped into six families: *CSLA*, *CSLB*, *CSLC*, *CSLD*, *CSLE*, and *CSLG* (Richmond and Somerville, 2000). All CSLs appear to be integral membrane proteins that contain features that are characteristic of processive GTs (Richmond and Somerville, 2001; Dhugga et al., 2004; Liepman et al., 2005). Also, all predicted *CSL* gene products contain the D,D,D,Q/RXXRW motif, which, together with topological features, indicates that they are involved in the synthesis of β-linked glycan polymers (Dhugga et al., 2004; Liepman et al., 2005). So far, this is borne out by in vitro activity assays of several heterologously expressed CSLs, all of which have been shown to synthesize (1→4)-β-linked products. For example, the CSLA family includes mannan synthases, while the CSLC family includes glucan synthases that are probably responsible for the construction of the backbone of xyloglucan (Dhugga et al., 2004; Liepman et al., 2005; Burton et al., 2006; Cocuron et al., 2007). Furthermore, *CSLF* genes in rice (*Oryza sativa*) were demonstrated to mediate the synthesis of (1→3),(1→4)-β-D-glucans (Burton et al., 2006). As expression systems and assays are optimized, it is likely that the products of the remaining CSLs will emerge. Possible products could include the backbones of xylan, noncrystalline cellulose, and the galactan side chains of pectin or arabinogalactan proteins (Liepman et al., 2005). Several Arabidopsis mutants with lesions in *CSL* genes have been described. The *kojak* mutant revealed that *CSLD3* is required for root hair growth, while *CSLA7* is required for pollen tube growth and embryogenesis (Favery et al., 2001; Wang et al., 2001; Goubet et al., 2003). In the *rat4* mutant, disruption of *CSLA9* results in the inhibition of *Agrobacterium tumefaciens*-mediated root transformation (Zhu et al., 2003). *CSLD5* is required for normal growth of the plant (Bernal et al., 2007). However, it has also been reported that for many *CSL*s, knockout plants do not have any obvious phenotypical defects (Richmond and Somerville, 2001). One reason for this may be functional redundancy within *CSL* families. However, it may also be the case that the activities of some *CSL*s may be spatially or temporally restricted, so that phenotypes that arise from disrupting their function are only apparent in particular cells or during a limited phase of development. Data from large-scale transcriptomics databases are providing detailed new insights into *CSL* expression and providing clues to where best to focus the analysis of *CSL* knockout plants. In this work, we have focused on the *CSLD* family, the closest one to the *CESA* genes, with 35% identity at the amino acid level (Richmond and Somerville, 2001). This family includes genes *CSLD1* through *CSLD6*, and most members of this family have highly distinctive expression profiles. We report here on the roles of *CSLD* genes in pollen tube and root hair development and discuss our findings in the wider context of the roles of *CSLD* genes in tip growth.

RESULTS

In Silico and Semiquantitative Reverse Transcription-PCR Expression Profiling of *CSLD* Genes

The meta-analyzer Genevestigator database, which collates data from Affymetrix ATH1 Arabidopsis arrays (https://www.genevestigator.ethz.ch/), was used to obtain an overview of the expression of the *CSLD* gene family (Supplemental Fig. S1). Four broad patterns of expression were observed. (1) *CSLD1* and *CSLD4* expression was very high in pollen, high in stamens, and moderate in flowers. Expression in all other tissues/organs was very low. (2) *CSLD2* and *CSLD3* expression was generally highest in root tissues but low in root tips. Both genes were also expressed at low or moderate levels in most other tissues/organs. (3) *CSLD5* was expressed at highest levels in hypocotyls and shoot apices but was also expressed at moderate levels in a range of other organs/tissues, including flowers, roots, and leaves. (4) *CSLD6* was expressed at near background levels in all tissues/organs. The expression of *CSLD* genes in response to environmental stress factors was analyzed using the "response-viewer" function of Genevestigator. This analysis revealed that the expression levels of *CSLD2* and *CSLD3* were increased by growth at reduced temperatures (data not shown). Furthermore, a more detailed analysis of the expression of *CSLD1* and *CSLD4* was obtained by interrogating a transcriptome database of pollen development (Honys and Twell, 2004). Neither *CSLD1* nor *CSLD4* was expressed above background levels during early pollen development (microspore stage). However, expression of both genes increased during pollen development and peaked in mature pollen (data not shown). Taken together, these data suggested that like *CSLD3*, *CSLD2* was likely to

be involved in root development, while *CSLD1* and *CSLD4* were likely to be involved in an aspect of late pollen development.

To extend the in silico analysis, we conducted semiquantitative reverse transcription (RT)-PCR of *CSLD1*, *CSLD2*, *CSLD3*, and *CSLD4* in wild-type Columbia (Col-0) plants (Supplemental Fig. S2). In agreement with in silico analysis, *CSLD2* and *CSLD3* were expressed to some extent in all plant organs examined, although the expression of *CSLD2* was somewhat lower than that of *CSLD3*. However, the expression of both of these genes was not notably higher in roots. The RT-PCR analyses of *CSLD1* and *CSLD4* were in broad agreement with the in silico analyses, and both genes were expressed at highest levels in flowers. However, *CSLD1* expression was also detected in roots and stems.

We further analyzed the cellular expression patterns of *CSLD2* and *CSLD3* in young seedlings by the use of plants expressing constructs containing a nucleus-targeted GFP:GUS fusion protein driven by the promoters of *CSLD2* or *CSLD3* (Supplemental Fig. S3). Confocal microscopy of 5-d-old seedlings carrying these constructs showed that both genes were expressed during the early and late stages of root hair development (Supplemental Fig. S3, A–D). However, *CSLD3* expression was generally much stronger than that of *CSLD2* in the distal portion of roots in trichoblasts at an early stage of root hair development (Supplemental Fig. S3, E–G).

Generation of *CSLD* Knockout Mutants

Insertional mutants of *CSLD1* (*csld1-1*), *CSLD2* (*csld2-1*), *CSLD3* (*csld3-2*), and *CSLD4* (*csld4-1*) were obtained from the SALK collection (Supplemental Fig. S4). The *csld3-2* mutant was so named to distinguish it from *csld3-1*, another previously described mutant with a lesion in *CSLD3* (Wang et al., 2001). In a separate forward genetic screen of T-DNA-mutagenized Arabidopsis seedlings, we identified a mutant with root hairs characterized by swollen bases and ruptured tips. Thermal asymmetric interlaced PCR confirmed a T-DNA insertion located in the first exon of *CSLD2*. This mutant was designated *csld2-2* (Supplemental Fig. S4). All mutants were generated in the Col-0 background, apart from *csld4-1*, which had a *quartet* (*qrt*) background. Homozygous lines were generated for all of the *CSLD2* and *CSLD3* mutants, and zygosity was confirmed by PCR (data not shown). Loss of expression of *CSLD2* and *CSLD3* in *csld2-1*, *csld2-2*, and *csld3-2* was confirmed by RT-PCR, as shown in Supplemental Figure S4F. A double homozygote mutant with insertions in both *CSLD2* and *CSLD3* (designated *csld2/3*) was also produced by crossing *csld2-2* and *csld3-2*. However, of more than 150 F1 selfed plants, no homozygous mutants of *CSLD1* or *CSLD4* were found. Therefore, both the *csld1-1* and *csld4-1* lines were maintained as heterozygous for insertions in these genes.

Mutants with Lesions in *CSLD2* Have a Defective Root Hair Phenotype That Is Distinct from Mutants with Lesions in *CSLD3*

Under the conditions we used, no aerial phenotype was observed for any of the mutants in *CSLD2* or *CSLD3*. The roots of 4-d-old wild-type Col-0 seedlings produced root hairs of varying lengths, as shown in Figure 1, A and D. In contrast, the root hairs of *csld2-1* seedlings were shorter than those of wild-type controls, and most had obvious visible deformities (Fig. 1, B and E). *csld2-2* had an identical defective root hair phenotype to *csld2-1* (data not shown). For comparison, three mutants with lesions in *CSLD3* were also examined, our own *csld3-2* and the previously described mutants *csld3-1* (Wang et al., 2001) and *kojak* (Favery et al., 2001). All three *CSLD3* mutants had identical root hair phenotypes, and the *csld3-1* phenotype is shown in Figure 1, C and F. In contrast to *csld2-1* and *csld2-2*, the *CSLD3* mutants produced few root hairs, and those hairs that were produced were usually ruptured at the tip soon after initiation. This was also the case for the double mutant *csld2/3*, which had an identical root hair phenotype to *csld3-2*, *csld3-1*, and *kojak* (Fig. 5E). The root hairs of *csld2-1* and *csld2-2* had deformities of various types, and representative examples are shown (Fig. 1, G–J). Some hairs appeared normal for much of their length but had severely bulged tip regions (Fig. 1G), whereas in others, the base of the root hair was bulged and the tip appeared normal (Fig. 1H). Other common phenotypes included multiple bulges along the length of the root hair (Fig. 1I) and root hair rupturing (Fig. 1J).

Detailed Analysis of Root Hair Rupturing in *csld2-1* and *csld3-2*

The rupture of *csld2-1* and *csld3-2* root hairs was analyzed in more detail using differential interference contrast (DIC) microscopy (Fig. 2). In both mutants, rupture was characterized by the loss of material that was presumably cytoplasm from the inside of cells. In *csld3-2*, rupture occurred soon after the initiation, as reported previously for *csld3-1* and *kojak* (Fig. 2, A and D). In contrast, if rupturing occurred in *csld2-1* root hairs, it was most commonly at a later stage when considerable hair growth had already occurred (Fig. 2, C and F). An additional notable difference between *csld2-1* and *csld3-2* was that in some cases, it appeared that root hair growth in *csld2-1* resumed after rupturing (Fig. 2, G and H). In some instances, the new growth apparently emanated from the tip of a previously ruptured hair, although it was not clear if this was a resumption of growth of the ruptured root hair or the growth of a new hair through the body of the original one (Fig. 2G). Where rupturing occurred on the flank of a root hair, new growth sometimes resumed at the basal region of the original one (Fig. 2H). In order to investigate this observation in more detail, hair growth in *csld2-1* and *csld3-2* was examined using

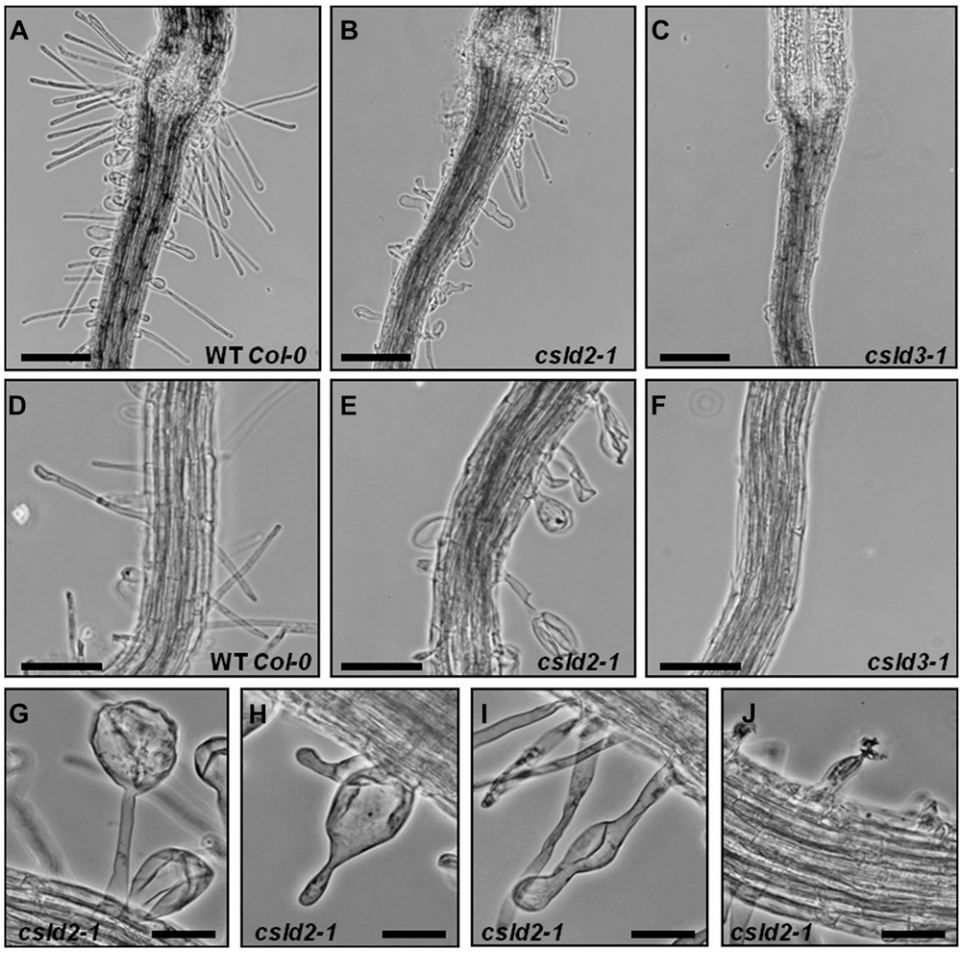

Figure 1. *csld2-1* has a defective root hair phenotype that is different from that of mutants with lesions in *CSLD3*. A to C, Images showing the root hypocotyl junction region of wild-type Col-0 (A), *csld2-1* (B), and *csld3-1* (C). D to F, Images of the middle portion of roots of wild-type Col-0 (D), *csld2-1* (E), and *csld3-1* (F). G to J, High-magnification images showing the range of aberrant root hair phenotypes observed in *csld2-1*. All images are of roots from 10-d-old *csld2-1* seedlings. Bars = 50 μm (A–F) and 25 μm (G–J).

time-lapse microscopy of living root hairs (Supplemental Movies S1–S5). In *csld2-1*, relatively mild ruptures, as evident by the appearance of a lesion at the surface of the hair cell, would sometimes be followed by temporary arrest of tip growth. During this period, cytoplasmic streaming in the root hair persisted, and in some cases a gradual swelling of the basal region of the root hair also occurred. Nevertheless, apparently normal tip growth was resumed (Supplemental Movie S1). In other cases, rupturing appeared to be more severe and material that was presumably cytoplasm was expelled from the tip of the root hair, as seen in the middle two root hairs in Supplemental Movie S2. However, even after these more severe ruptures, tip growth was still observed to resume after a period of growth arrest (Supplemental Movie S2). When rupturing was very severe, as was evident by massive cytoplasmic discharge, cytoplasmic streaming ceased and tip growth did not recover (Supplemental Movie S3). *csld2-2*, which we isolated from a forward genetic screen, displayed identical root hair swelling and rupturing phenotypes as *csld2-1* (data not shown). As with *csld2-1*, the severity of rupturing of *csld3-2* hairs appeared to vary. For example, in some cases, relatively little cytoplasm was released and cytoplasmic streaming continued (Supplemental Movie S4). In other cases, more cytoplasm was apparently released and cytoplasmic streaming ceased altogether (Supplemental Movie S5).

We measured the frequency of root hair growth resumption after tip rupture from several time-lapse movies of growing root hairs located at 500 to 700 μm from the primary root tips of 3- to 4-d-old *csld2-1* seedlings. Of a total of 157 root hairs from 15 independent time-lapse sequences spanning 1 h of growth, we observed that 16% of the root hairs ruptured, but rupturing was soon followed by tip growth resumption. Irrespective of the severity of rupturing, and in contrast to *csld2-1*, resumption of tip growth was never observed in *csld3-2*.

csld2-1 and *csld2-2* Root Hairs Have Altered Wall Ultrastructure But Normal Cellular Patterning in Roots

Expression data indicated that both *CSLD2* and *CSLD3* are expressed to some extent throughout roots. However, the *CSLD3* mutants *kojak* and *csld3-1* have been reported to have no abnormalities in cell types other than root hairs (Favery et al., 2001; Wang et al., 2001). In order to investigate if this was also the case

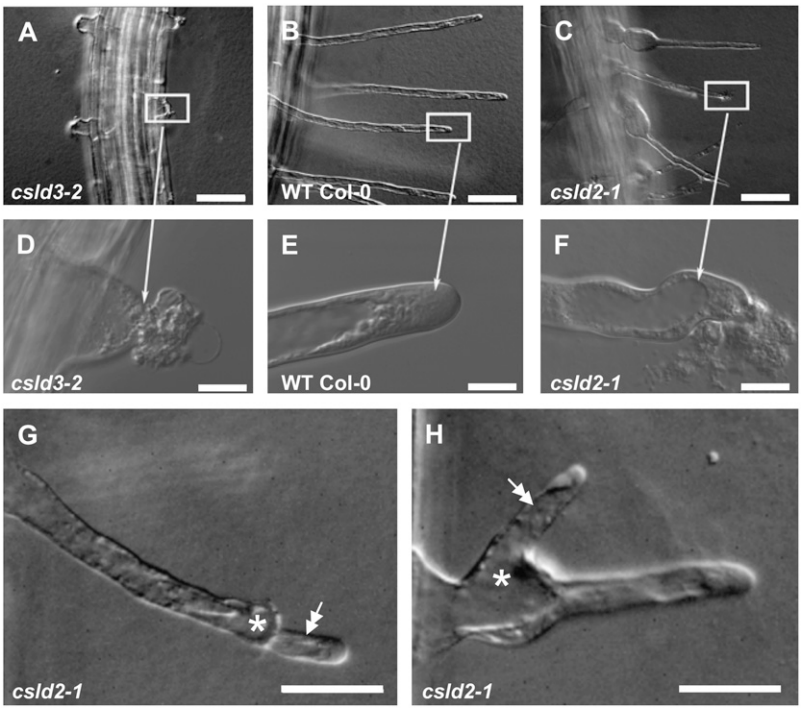

Figure 2. Tip rupture in *csld2-1* and *csld3-2* and regrowth in *csld2-1*. A to F, DIC images of root hairs from *csld3-2* (A and D), wild-type Col-0 (B and E), and *csld2-1* (C and F). The rupturing of root hair tips and loss of cytoplasm are visible in both *csld3-2* (D) and *csld2-1* (F). G and H, In *csld2-1*, new root hair growth was apparent after rupturing of hairs both at the tip (G) and flank (H) regions. Double arrows indicate new root hair growth. Asterisks indicate the area of rupture. Bars = 50 μm (A–C), 10 μm (D–F), and 20 μm (G and H).

for *csld2-1*, sections were taken through roots of 10-d-old *csld2-1* seedlings and equivalent wild-type Col-0 seedlings (Fig. 3, A–C). Cell number and cellular patterning in the cortex and epidermis were normal in *csld2-1*, nor were defects observed in the stele. Excessive bulging was apparent in many of the *csld2-1* root hairs sectioned, but other regions of *csld2-1* trichoblasts appeared normal, and bulging did not intrude into other epidermal or cortical cells (Fig. 3B). At higher magnification, it was apparent that in many cases, the cell walls of *csld2-1* root hairs appeared variable in thickness (Fig. 3C).

In order to investigate cell wall ultrastructure in more detail, sections through *csld2-1*, *csld2-2*, *csld3-2*, and wild-type Col-0 root hairs were examined using transmission electron microscopy. Walls were examined at various positions along root hairs from base to tip, and representative examples are shown in Figure 3, D to L. The walls of wild-type Col-0 hairs had a dense fibrillar appearance and had a consistent thickness of approximately 0.25 μm along the length of root hairs (Fig. 3, D–F). In contrast, the walls of *csld2-1* root hairs varied in thickness from approximately 0.2 to 0.6 μm (Fig. 3, G–I). In regions where *csld2-1* root hair walls were thickened, they also had a more diffuse appearance, as shown in Figure 3G. This variability in thickness and more diffuse fibrillar network were also apparent in the walls of *csld2-2* and *csld3-2* root hairs (Fig. 3, K and L).

csld2-1 Root Hairs Have a Disrupted Cytoskeletal Organization

It is known that there is an intimate relationship between cell wall formation and cytoskeletal organization (Wasteneys, 2004; Paredez et al., 2006). Given the disrupted cell wall architecture and severe morphological defects in root hairs of *csld2-1*, we were interested to see if cytoskeletal organization was also affected. *csld2-1* was crossed with Arabidopsis plants expressing GFP reporters that bind to microtubules (35S::GFP-MBD; Marc et al., 1998) or actin filaments (35S::GFP-ABD2-GFP; Wang et al., 2008). We observed that the organization of both components of the cytoskeleton was disrupted in *csld2-1* root hairs but that the severity of disruption depended on the growth status and shape of the root hair. For example, in the base of wild-type root hairs, F-actin and microtubules were arranged in a predominantly longitudinal fashion (Fig. 4, A and C). In contrast, in the swollen bases of *csld2-1* root hairs, the orientation of F-actin and microtubules was less organized (Fig. 4, B and D). Tip regions of wild-type root hairs were characterized by longitudinal F-actin arrays that did not extend to the apex of hairs (Fig. 4E). In *csld2-1*, although F-actin was disorganized in bulged root hair bases, in tip regions with normal morphologies F-actin had a similar predominantly longitudinal orientation as wild-type Col-0; also like wild-type Col-0, the F-actin arrays did not extend to the apex of hairs (Fig. 4G). However, in cases where the tips of *csld2-1* root hairs were swollen or had ruptured, the F-actin arrays were disorganized and did extend to the root hair apices (Fig. 4I). Similar observations were also made for microtubules: in wild-type and nonruptured *csld2-1* hairs, microtubules had a predominantly longitudinal orientation and did not extend to root hair apices (Fig. 4, F–H), while in swollen or ruptured *csld2-1* hairs, microtubules had a less organized orientation and did extend to the hair

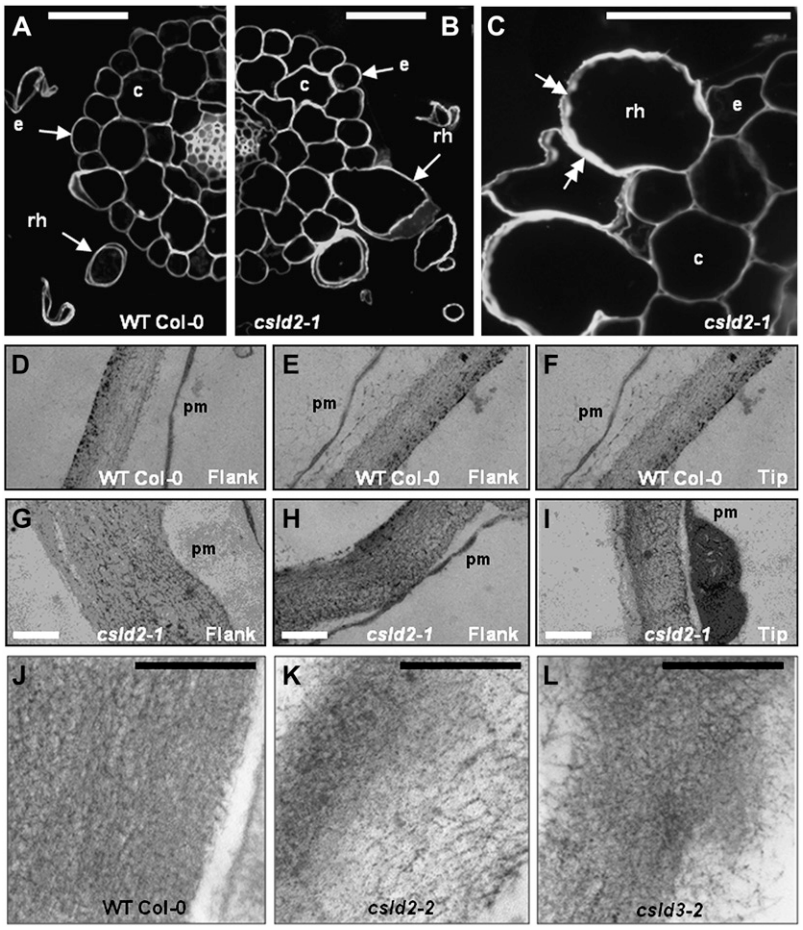

Figure 3. The cellular anatomy of *csld2* is normal apart from the altered root hair phenotype. A and B, Images showing resin-embedded roots from 12-d-old wild-type Col-0 (A) and *csld2-1* (B) seedlings. Overall cellular patterning was normal in *csld2-1* roots, and apart from root hairs (rh), all cells had normal morphologies, including atrichoblast epidermal cells (e) and cortical cells (c). C, High-magnification image of a section through a root of *csld2-1* showing root hair, atrichoblast epidermal cells, and cortical cells. Double arrows indicate the region of root hair walls that are thickened or of variable thickness. D to L, Transmission electron microscopy of cell walls from wild-type Col-0 (D–F and J), *csld2-1* (G–I), *csld2-2* (K), and *csld3-2* (L). Images were taken of equivalent flank (D, E, G, and H) and tip (F and I) regions of wild-type Col-0 and *csld2-1* root hairs. In J to L, note the diffuse appearance of *csld2-2* and *csld3-2* walls compared with wild-type Col-0 walls. Bars = 50 μm (A–C), 0.2 μm (D–I), and 0.1 μm (J–L).

apex (Fig. 4J). The bases of some root hairs of *csld2* did not bulge. In these nonbulged bases, the organization of F-actin and microtubules resembled that of wild-type roots (data not shown).

The Defective Root Hair Phenotypes of *csld2-1* and *csld3-2* Are Partially Rescued by Growth at Reduced Temperature

In silico expression analysis had revealed that the expression of both *CSLD2* and *CSLD3* is increased by growth at a reduced temperature, and we were interested to see if this increased expression had an effect on the root hair phenotypes of *csld2-1* and *csld3-2*. Root hair morphologies (Fig. 5, A–E) and length (Fig. 5F) were compared for seedlings grown at 25°C and 15°C. At 25°C, *csld2-1* root hairs displayed the characteristic phenotype described previously, including swelling at the hair base and tip rupturing (Fig. 5A). However, when *csld2-1* was germinated and grown at 15°C for 6 to 9 d, these defects were largely reduced: swelling of hair bases and tip rupturing were rare, and root hairs grew to a similar length as wild-type controls (Fig. 5, B and F). The phenotype of *csld3-2* was also partially rescued by growth at 15°C, although to a lesser extent than for *csld2-1*. At 25°C, the usual severe defects in *csld3-2* root hairs were observed (Fig. 5C), but when grown at 15°C, rupturing of *csld3-2* hairs was delayed such that many root hairs grew to approximately half the length of wild-type controls (Fig. 5, D and F). In all previous analyses, the double mutant *csld2/3* appeared to have an identical defective root hair phenotype as *csld3-2* and no additional phenotypical changes. Interestingly, though, unlike *csld3-2*, the root hair defects in *csld2/3* were not rescued by growth at 15°C (Fig. 5, C, E, and F).

As noted, in silico analysis showed that *CSLD2* and *CSLD3* were induced by low temperatures, and this could explain the partial suppression of the *csld2* and *csld3* root hair phenotypes when grown at 15°C. To verify the in silico data, we conducted semiquantitative RT-PCR of *CSLD2* and *CSLD3* expression in 6-d-old wild-type, *csld2-1*, *csld3-2*, and double *csld2/3* mutant roots grown at 25°C and 15°C (Fig. 6A). Consistent with the in silico analysis, expression of *CSLD2* and *CSLD3* was higher in roots of wild-type plants grown at 15°C compared with 25°C. Furthermore, *CSLD3* expression was higher in *csld2-1* at 15°C compared with 25°C. However, *CSLD2* expression in *csld3-2* mutants grown at 15°C was not increased in seedlings grown at 15°C. We also analyzed the effect of temperature on *CSLD2* and *CSLD3* expression by the use of

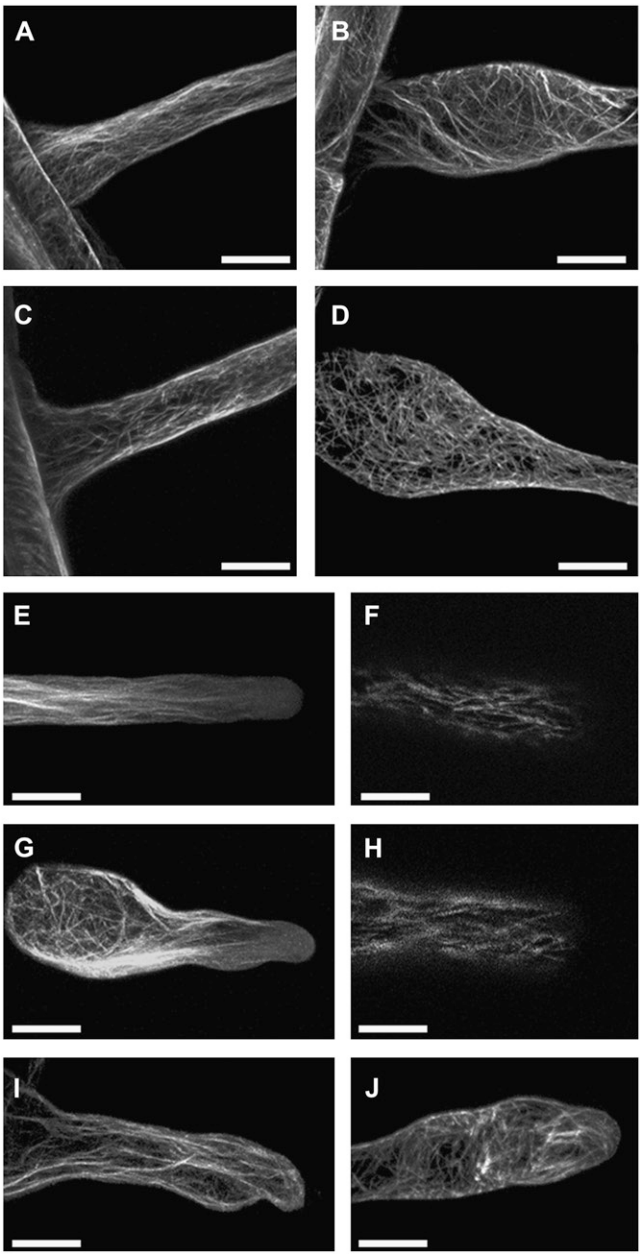

Figure 4. Microtubule and F-actin organization is disrupted in living *csld2-1* root hairs. A to D, F-actin (A and B) and microtubules (C and D) in the base of wild-type Col-0 (A and C) and *csld2-1* (B and D). E to J, F-actin organization in the tip regions of wild-type Col-0 (E) and *csld2-1* (G and I), and microtubule organization in the tip regions of wild-type Col-0 (F) and *csld2-1* (H and J). F-actin and microtubules were visualized by GFP-ABD2-GFP and GFP-MBD2 fusions, respectively. Bars = 20 μm.

plants expressing the GUS gene driven by the promoters of *CSLD2* or *CSLD3* (Fig. 6B). Using this approach, the expression of *CSLD2* was not notably elevated at 15°C compared with 25°C, but the expression of *CSLD3* was markedly higher at the lower temperature.

The *csld-2* Root Hair Phenotype Is Rescued by Complementation with *CSLD2* Driven by Its Own Promoter

In order to determine if the defective root hair phenotype of *csld2-1* was indeed due to the mutation of the *CSLD2* gene, *csld2-1* was transformed with a wild-type version of the *CSLD2* gene driven by its own promoter. As shown in Figure 7, the root hairs of these complemented plants were identical in appearance and length to the root hairs of wild-type Col-0.

csld4-1 Has Normal Pollen Grain Morphology But Reduced Pollen Tube Germination

The facts that *CSLD1* and *CSLD4* were both expressed at high levels in pollen and that no homozygous plants were obtained in the F1 generation suggested that both genes may have roles in pollen development and/or pollen tube germination. In order to investigate if *csld4-1* had defects in pollen grain morphology, sections through resin-embedded anthers from *csld4-1* and *qrt* were stained with toluidine blue (Fig. 8, A and C). No differences were observed between *csld4-1* and *qrt* with respect to the morphology and cellular anatomy of anthers, the number of pollen grains (data not shown), or the overall shape or size of pollen grains (Fig. 8, A and C). At higher magnifications of toluidine blue-stained sections, the pollen coat and intine were clearly visible, and again there were no obvious differences between *csld4-1* and *qrt* (Fig. 8, A and C).

Pollen tube germination in *csld4-1* and *qrt* was assessed using in vitro germination assays (Fig. 8, B and D). The *qrt* mutant is defective in pectin degradation, and pollen grains in *qrt* adhere together rather than separating as usual after meiosis completion (Rhee and Somerville, 1998). By generating *csld4-1* in a *qrt* background, we were able to examine pollen tube germination in relation to quartet genotype, since in each heterozygote *csld4-1* quartet, two of the grains have a wild-type version of *CSLD4* and two have the mutated version. By visual examination, it was clear that the overall extent of pollen tube germination was greater in *qrt* compared with *csld4-1* (Fig. 8, B and D). Moreover, whereas up to four pollen tubes were observed to emerge from *qrt* quartets, a maximum of two were produced by *csld4-1* quartets.

Quantification of Pollen Tube Germination in *csld1-1*, *csld2-1*, and *csld4-1*

Total pollen tube germination rates were determined for *csld1-1*, *csld4-1*, and *csld2-1* (control) by scoring the in vitro germination assays (Fig. 9A). Germination was reduced by approximately 50% in *csld1-1* and *csld4-1* compared with wild-type Col-0 and *qrt*, respectively. However, the germination rate of pollen from *csld2-1* did not significantly differ from that of wild-type Col-0 control pollen. The number of

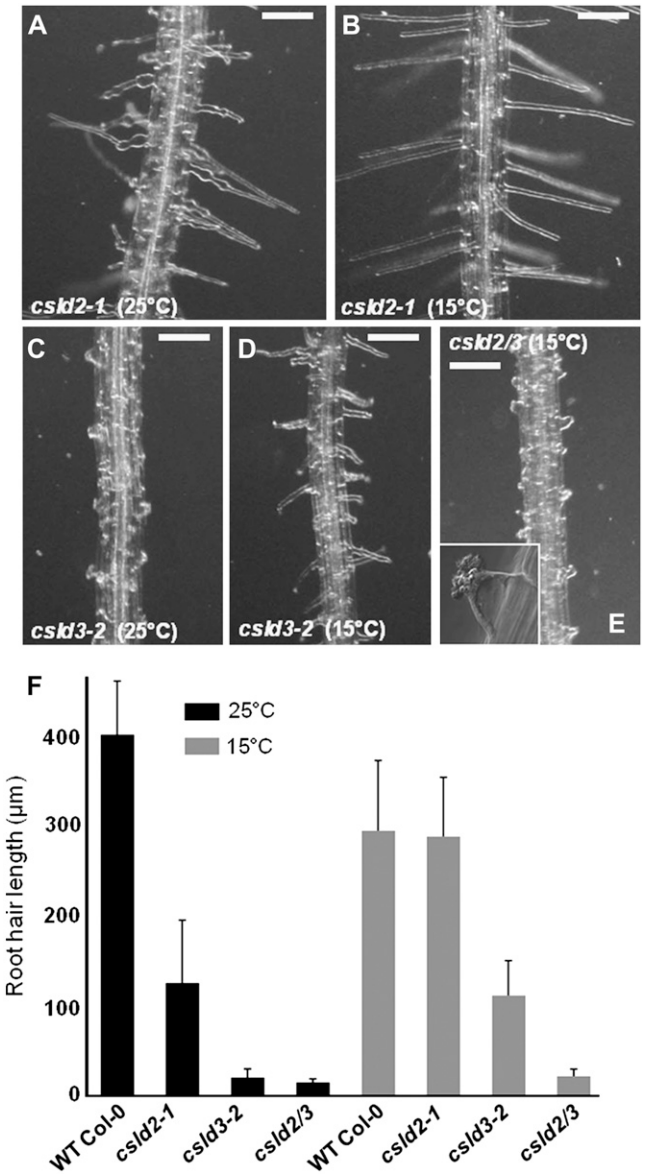

Figure 5. The altered root hair phenotypes in *csld2-1* and *csld3-2* are partially rescued by growth at reduced temperature. A to E, *csld2-1* (A and B) and *csld3-2* (C and D) were grown at 25°C (A and C) or 15°C (B and D). Growth at 15°C resulted in partial rescue of root hair phenotypes in both *csld2-1* and *csld3-2*. However, the phenotype of a double mutant with lesions in *CSLD2* and *CSLD3* (*csld2/3*) was not rescued by growth at 15°C (E). The inset in E shows a high-magnification image of a ruptured root hair of the *csld2/3* double mutant. F, Quantification of root hair length in *csld2-1*, *csld3-2*, and *csld2/3*. The graph shows average root hair length of 10 seedlings. WT, Wild type. Error bars indicate SE. Bars in A to E = 100 μm.

pollen tubes that germinated from individual quartets was also determined for *qrt* and *csld4-1* (Fig. 9B). In both *qrt* and *csld4-1*, of the quartets that germinated, most produced one or two pollen tubes. However, whereas some *qrt* quartets produced three or four pollen tubes, *csld4-1* quartets produced a maximum of two, confirming the visual examination shown in Figure 8. Moreover, the segregation of the insertional mutations in *csld1-1* and *csld4-1* was analyzed by a series of crosses between mutant and wild-type plants (Table I). The segregation ratio for self crosses of both *csld1-1* and *csld4-1* was approximately 1:1, suggesting a disorder in gametophytic transmission rather than a zygotic lethality of the mutation. We then further analyzed the transmission of the mutation in *csld4-1* by performing reciprocal crosses with *qrt* and analyzed the progeny for BASTA resistance. Male transmission was abrogated by the mutation in *csld4-1*, whereas female transmission was not affected.

In order to determine if the mutation of the *CSLD4* gene was indeed responsible for the distorted transmission ratios we observed, segregation analysis was also performed on *csld4-1* plants that had been transformed with the *CSLD4* gene driven by its own promoter. The T1 progeny of a self-pollinated plant segregated in a 3:1 ratio for BASTA resistance, confirming that the mutation in *CSLD4* was responsible for the abrogated male transmission (Table I).

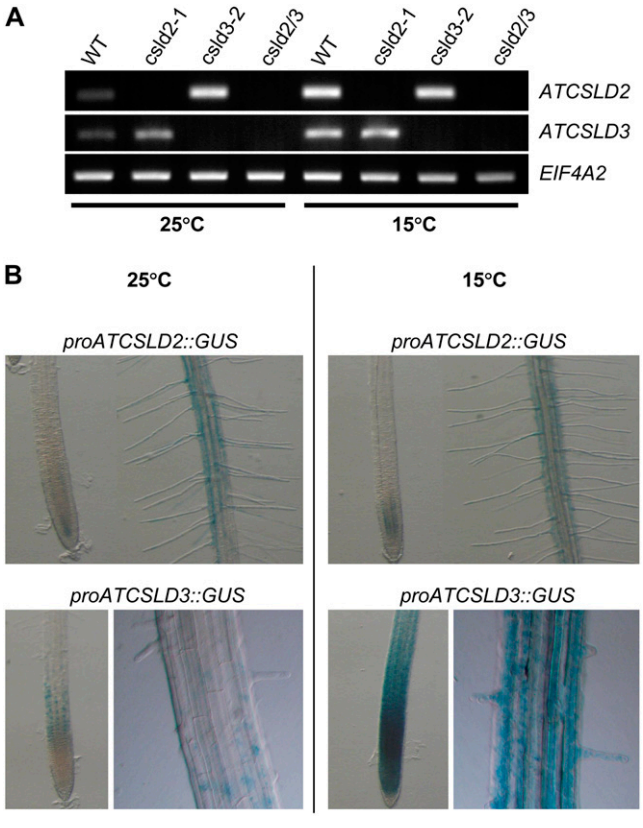

Figure 6. Effect of reduced temperature on *CSLD2* and *CSLD3* expression. A, RT-PCR analysis of *CSLD2* and *CSLD3* genes in the wild type (WT), *csld2-1*, *csld3-2*, and *csld2/3* mutants. RNA was isolated from roots of 6-d-old seedlings grown at 25°C or 15°C. Arabidopsis translation initiation factor EIF4A2 was used as a constitutive expression control. B, Histochemical analysis of GUS expression in roots of 6-d-old wild-type seedlings carrying constructs of GFP::GUS driven by the *CSLD2* or *CSLD3* promoter and grown at 25°C or 15°C.

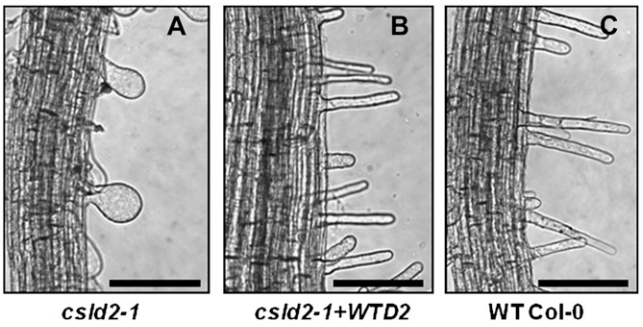

Figure 7. The altered root hair phenotype of *csld2-1* was restored by transformation with wild-type *CSLD2* driven by its own promoter. Images show the root hair morphologies in *csld2-1* (A), *csld2-1* transformed with the wild-type *CSLD2* gene driven by its own promoter (*csld2-1+WTD2*; B), and wild-type Col-0 (C). All images are of roots from 10-d-old seedlings. Bars = 50 μm.

Subcellular Localization of CSLD2, CSLD3, and CSLD4

Previous work to determine the subcellular localization of CSLD3 (KOJAK), using a C-terminal fluorescent tag, concluded that this protein is localized in the endoplasmic reticulum (Favery et al., 2001). We found that CSLD5 also appeared to be endoplasmic reticulum localized when a C-terminal florescent tag was used. However, when CSLD3 or CSLD5 was tagged at the N terminus, both proteins were localized in the Golgi apparatus (Bernal et al., 2007). Proteomic LOPIT (for Localization of Organelle Proteins by Isotope Tagging) analysis recently demonstrated that CSLD2 and CSLD3 are in fact localized in the Golgi apparatus (Dunkley et al., 2006), and a considerable body of evidence indicates that most GTs involved in cell wall biosynthesis are located either at the plasma membrane (in the case of the CESAs) or in the Golgi apparatus. Together, these data suggest that N-terminal, rather than C-terminal, tagging is more likely to reliably report the location of CSLD proteins. With this in mind, we conducted subcellular localization experiments of CSLD2 and CSLD4 using yellow fluorescent protein (YFP) fused at the N terminus together with the STtmd-GFP Golgi apparatus marker for comparison (Fig. 10). The locations of YFP-CSLD2, YFP-CSLD3, and YFP-CSLD4 were similar to that of STtmd-GFP; therefore, these results confirmed the previous findings for CSLD2 and CSLD3 and indicate that CSLD4 is likewise localized in the Golgi apparatus. The functionality of the YFP-CSLD3 fusion was demonstrated by the fact that the *csld3-2* phenotype was rescued by complementation with this construct (Supplemental Fig. S5).

DISCUSSION

Tip growth is an important and highly specialized cellular growth process carried out in certain cells, including root hairs, pollen tubes, fungal hyphae, moss protonema, and fern rhizoids (Parton et al., 2000; Carol and Dolan, 2002; Cole and Fowler, 2006). In contrast to the growth of most plant cells, during tip growth secretory vesicles containing cell wall components are targeted exclusively to the growing apex of cells (Cole and Fowler, 2006). We have shown here that *CSLD1* and *CSDL4* are required for pollen tube development and that *CSLD2* is required for normal root hair formation. The phenotypes observed for plants with mutations in these genes were broadly consistent with expression profiles determined by in silico, GFP, RT-PCR, and GUS analyses, and the results from complementation experiments also supported the direct involvement of these genes in pollen tube and root hair growth.

Although the in silico expression profiles of *CSLD2* and *CSLD3* were nearly identical, it was clear from more detailed analysis that they in fact have subtly different expression patterns, and this is reflected in the distinct phenotypes of mutants with lesions in the genes. While *CSLD3* is required during the transition from root hair initiation to tip growth proper, *CSLD2* appears to be required at a later stage of development during tip growth itself. This might be partly explained by the subtle differences in timing of the expression of these genes in root hairs, as indicated by GFP analysis that showed higher *CSLD3* expression in the distal part of roots compared with *CSLD2*. It is possible that there are other differences in the expression of these genes that were not revealed by our experiments.

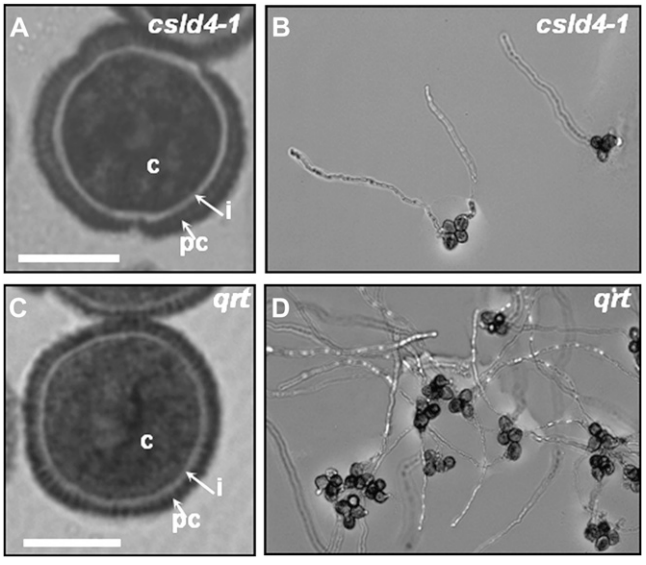

Figure 8. *csld4-1* pollen has a normal morphology but reduced pollen tube germination. A and C, Resin-embedded pollen from *csld4-1* (A) and *qrt* (C) was sectioned and stained with toluidine blue. B and D, Images from in vitro germination assays showing quartets of pollen grains and pollen tubes from *csld4-1* (B) and *qrt* (D). c, Cytoplasm; i, intine; pc, pollen coat. Bars in A and C = 1 μm.

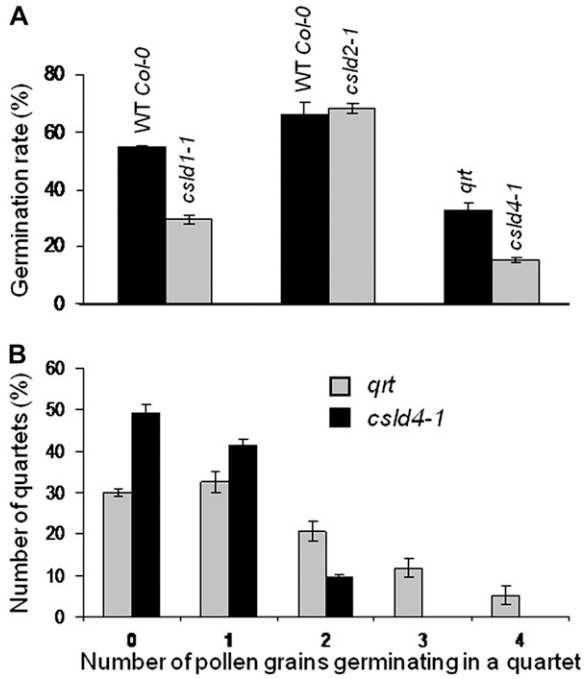

Figure 9. Quantification of pollen tube germination rates in *CSLD* mutants. A, Quantification of the in vitro germination rate of pollen tubes from *csld1-1*, *csld2-1*, and *csld4-1* compared with wild-type (WT) Col-0 and *qrt*. Note that pollen tube germination was normal in *csld2-1*. B, Quantification of the number of pollen tubes germinating from quartets. In *csld4-1*, the maximum number of pollen tubes germinating from a single quartet was two, whereas up to four tubes germinated from the *qrt* quartet. Error bars indicate SE among three independent experiments with 80 samples each.

The observation that the *csld2/3* homozygous double mutant has the same phenotype as *csld3-2* under normal growth conditions indicates that *CSLD3* is epistatic to *CSLD2*. Moreover, the partial rescue of the *csld2-1* and *csld3-2* phenotypes, when grown at 15°C, suggests that there may be partial functional redundancy between these genes. Thus, it may be the case that increased expression of *CSLD3* at 15°C may be sufficient to partially compensate for the lack of the *CSLD2* in *csld2-1*, and likewise for *CSLD2* in *csld3-2*. This hypothesis is also supported by the fact that the phenotype of *csld2/3*, in which both genes are defective, was not rescued by growth at 15°C. While the *csld2-1* phenotype was restored to nearly normal by growth at 15°C, the effect was less complete for *csld3-2*. This is consistent with the fact that although in silico expression indicated that *CSLD2* expression was elevated by reduced temperature growth, GUS and RT-PCR analyses did not. This suggests that reduced temperature has only a slight effect on *CSLD2* expression, which could account for the phenotypic compensation observed in *csld3* mutants.

It is conceivable that the phenotypic recovery at reduced temperature resulted from altered physical properties of root hairs and/or growth medium at 15°C that rendered root hairs less susceptible to developing growth defects. However, if this were the case, then it would be expected that the *csld2/3* double mutant would also show a similar phenotype at reduced temperature to *csld3-2*. A partial redundancy between *CSLD2* and *CSLD3* also seems plausible in the light of evidence that GTs within a given CSL family all appear to catalyze the synthesis of the same polysaccharide (Dhugga et al., 2004; Liepman et al., 2005; Cocuron et al., 2007). Both *CSLD2* and *CSLD3* are expressed to some extent in many Arabidopsis organs and tissues, but apart from root hair defects there were no obvious phenotypes in *csld2-1*, *csld3-2*, or *csld2/3*. This may suggest that another *CSLD* gene(s) can compensate for the loss of *CSLD2* and *CSLD3* in locations other than roots. If this is the case, then *CSLD5* and *CSLD1* are the most likely candidates, since their expression profiles overlap with those of *CSLD2* and *CSLD3* (Bernal et al., 2007; Supplemental Fig. S2).

In both *csld1-1* and *csld4-1*, approximately half of the pollen grains failed to produce pollen tubes at all, indicating that *CSLD1* and *CSLD4* are required at a very early stage of pollen tube growth. However, it is important to add that the data presented here do not completely rule out the possibility that these mutations affect a pregermination, rather than a postgermi-

Table I. *Segregation analysis of mutations in CSLD1 and CSLD4*

Cross	Progeny with Insertion[a]	Progeny without Insertion[b]	Ratio[c]	χ^{2d}	P^e
d4/D4[f] *qrt/qrt*♀ × *d4/D4 qrt/qrt*♂	88	93	1:1	0.138	0.710
d1/D1♀ × *d1/D1*♂	86	103	1:1	1.529	0.216
d4/D4 qrt/qrt♀ × *D4/D4 qrt/qrt*♂	27	30	1:1	0.158	0.691
D4/D4 qrt/qrt♀ × *d4/D4 qrt/qrt*♂	0	120	0:1	0	1
d4/D4 +WTD4♀ × *d4/D4* +WTD4♂	59	20	3:1	0.004	0.948

[a]BASTA-resistant plants in crosses with *csld4-1* and progeny positive for the PCR analysis in crosses with *csld1-1*. [b]BASTA-susceptible plants in crosses with *csld4-1* and progeny negative for the PCR analysis in crosses with *csld1-1*. [c]Segregation ratio for which χ^2 values were calculated. [d]χ^2 values calculated with expected/observed values for the segregation ratios shown in the previous column. [e]Probability associated to the χ^2 value shown in the previous column with 1 degree of freedom. Probability values obtained indicate that no difference can be detected between observed and expected values in each experiment. [f]*d4/D4*, Plants heterozygous for the *csld4-1* mutation.

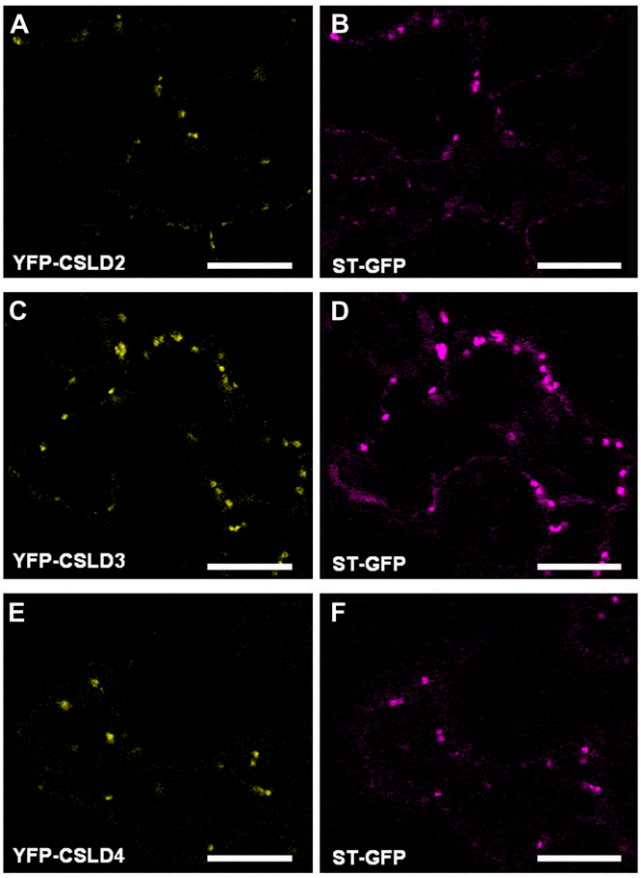

Figure 10. Subcellular localization of CSLD1 and CSLD4. Fluorescently tagged versions of CSLD2 (A), CSLD3 (C), and CSLD4 (E) in which YFP was fused to the N termini were expressed in *Nicotiana benthamiana* leaves and visualized using confocal laser-scanning microscopy. The Golgi apparatus marker STtmd-GFP (ST-GFP) was also expressed in *N. benthamiana* leaves (B, D, and F). Bars = 15 μm.

nation, process. *CSLD1* and *CSLD4* showed no signs of redundancy, since both single mutants showed abnormalities in the male gametophyte. This might be due to small differences in gene expression not detected with the experimental procedures used. Alternatively, it might be the case that functional cooperation is required by the GTs encoded by *CSLD1* and *CSLD4* in order to fulfill their functions.

One remarkable feature of *csld2-1* that was revealed by time-lapse microscopy was that root hair growth could recover after hair rupturing, even after an apparent loss of cytoplasm. Several root hair mutants, for example, *tip1* and *cow1*, have been reported in which multiple hairs develop from a single trichoblast (Grierson et al., 1997; Böhme et al., 2004). However, in these mutants, rupturing was not observed and the multiple hairs were proposed to be the result of defects in the mechanisms that regulate hair number (Grierson et al., 1997). Root hair number was normal in *csld2-1*, and hair regrowth appeared to be a repair mechanism. In most plant cells, rupture of the tonoplast to the extent that cytoplasm is released results in cell death. Indeed, in some cells, tonoplast rupture is the first event in programmed cell death (Gunawardena et al., 2004). One notable example of where recovery does occur after rupturing is in fern gametophyte rhizoids (Parton et al., 2000). These tip-growing cells are very similar in appearance to angiosperm root hairs, and many aspects of their cytology during tip growth are also similar. A detailed study of *Dryopteris affinis* rhizoids showed that new tip growth occurred after mechanically induced rupturing and loss of cellular material (Parton et al., 2000). In both *D. affinis* rhizoids and *csld2-1* root hairs, recovery was observed in cells that had already undergone active tip growth. Since regrowth after rupture did not occur in *csld3-2*, this may indicate that the ability to recover is linked to a certain developmental phase in tip-growing cells. Rhizoids and root hairs are both adapted to anchorage and nutrient uptake, and it may be the case that a capacity for recovery is the result of convergent evolution in response to common environmental challenges. It has also been suggested that there may be an ancient evolutionary link between sporophyte root hairs and gametophyte rhizoids, and their shared ability to recover after rupture may reflect this (Parton et al., 2000).

Our results add to a compelling body of evidence that implicates *CSLD* genes in tip growth across the plant kingdom. The rice *CSLD1* gene appears to be a functional ortholog of *CSLD3*, and root hair growth is impaired when *CSLD1* is disrupted in rice (Kim et al., 2007). The *CSLD1* gene is abundantly expressed in *Nicotiana alata* pollen tubes, and *CSLD* expression is high in tip-growing moss protonema cells. In contrast to higher plants, in which tip grow is limited to relatively few cells, in moss it is a prominent cellular growth mechanism of the plant body (Roberts and Bushoven, 2007). It is significant, therefore, that in *Physcomitrella patens*, 46% of all *CESA* superfamily ESTs are *CSLD*s, compared with only 10% in Arabidopsis (Roberts and Bushoven, 2007). Intriguingly, *CSLD5* does not obviously fit this pattern. *CSLD5* is expressed at highest levels during stem growth, and the *csld5-1* mutant has reduced stem growth but no visible defects in tip-growing cells (Bernal et al., 2007). It may be the case that *CSLD5* is not involved in tip growth, but it is worth noting that GUS expression analysis of *CSLD5* indicated a role in xylem development, and xylem fibers grow by invasive tip growth (Mellerowicz et al., 2001; Samuga and Joshi, 2004). In this regard, it may also be significant that the *CSLD2* gene in poplar (*Populus* spp.) that shares 90% similarity with *CSLD3* is expressed in developing xylem, and it has been proposed to be involved in the control of fiber length (Samuga and Joshi, 2004).

The most straightforward explanation of the phenotypes we observed is that the product of CSLD GTs is a structural component of cell walls, and disrupting or reducing the level of this component leads to wall weakening, basal swelling, and tip rupture. The transmission electron microscopy images shown in Figure 3

indicate that one aspect of reduced wall integrity may be a reduction in the cohesion of the mesh-like wall matrix that leads to a less dense appearance. It is worth noting that the LXR1 and LXR2 Leu-rich repeat extensins, which probably have structural roles in cell walls, are also involved in maintaining normal root hair growth. Similar to *csld2-1* and *csld2-2*, root hairs of *lxr1* mutants rupture at the tip and exhibit basal swelling (Baumberger et al., 2001). Root hairs of double *lxr1/lxr2* mutants also have irregular wall thickness and density, which resemble the cell wall architecture of *csld2-1* and *csld2-2* (Baumberger et al., 2001). Recently, plants that are deficient in xyloglucans resulting from disruptions in genes encoding xylosyltransferases produced root hairs with swollen bases that resembled *csld2* mutants (Cavalier et al., 2008). It is highly likely that all CSLD GTs are involved in the synthesis of a β-linked polysaccharide, and although we do not know which polysaccharide this is, the evidence to date suggests a β-glucan. One clue comes from the similarity of the *CSLD*s to other GT genes that are known to catalyze β-glucan synthesis. Of all the *CSL*s, the *D* family members are the most similar to the *CESA*s (Richmond and Somerville, 2000). Also, phylogenetic analysis of *CSL* genes in rice suggests that the *CSLF* genes that are involved in (1→3),(1→4)-β-D-glucan synthesis may have diverged from the *CSLD* family (Buckeridge et al., 2004; Keegstra and Walton, 2006). Additional evidence comes from analysis of *N. alata* pollen tubes that contain (1→3)-linked and (1→4)-linked β-glucans and α-linked pectic polymers (Doblin et al., 2001). The presence of the (1→3)-β-glucan can be accounted for by an abundantly expressed putative callose synthase, *NaGsl1*, but no significant expression of any *CESA* genes was detected. However, a *CSLD* gene, *NaCslD1*, is abundantly expressed and is likely to be involved in the synthesis of the (1→4)-β-glucan (Doblin et al., 2001). We have shown here that CSLD2, CSLD3, and CSLD4 proteins are localized in the Golgi apparatus, and this is also the case for CSLD5 (Bernal et al., 2007). Moreover, it was recently shown that CSLD2 is an integral Golgi membrane protein (Zeng and Keegstra, 2008). With this in mind, it seems that if CSLD GTs do synthesize a β-glucan, it is distinct from crystalline cellulose, which is made by the plasma membrane-bound CESAs. It is possible that CSLDs synthesize another, possibly noncrystalline, form of β-glucan. Support for this possibility comes from Arabidopsis suspension cultured cells that were habituated to grow in the herbicide isoxaben that specifically disrupts CESA activity. *CSLD5* was highly up-regulated in these cells, and their walls contained an apparently amorphous and glucanase-sensitive β-glucan (Manfield et al., 2004).

The extensive distortion to the cytoskeleton we observed in *csld2-1* and *csld3-2* root hairs suggests that disruption of *CSLD* function also has secondary effects. There is substantial evidence of an intimate and reciprocal link between the cortical cytoskeleton and cellulose synthesis (Wasteneys, 2004; Emons et al., 2007). This relationship is manifest both in cellulose synthase mutants that have disrupted cytoskeletal organization and in cytoskeleton mutants that have disrupted cellulose deposition (Burk and Ye, 2002; Chu et al., 2007; Paredez et al., 2008). However, this relationship does not involve absolute mutual dependence. For example, in *mor1-1* root cells, cellulose microfibrils are correctly deposited even after disruption of cortical microtubules (Sugimoto et al., 2003; Wasteneys, 2004). One explanation of our results, given that *CSLD2* and *CSLD3* are very unlikely to be directly involved in the synthesis of either crystalline cellulose or the cytoskeleton, is that the glycan product of the GTs encoded by these genes is associated directly or indirectly with cellulose microfibrils. If so, then disruption of this glycan may also disrupt microfibril deposition and, hence, cytoskeletal stability and alignment. However, a more subtle explanation can be suggested based on the fact that microtubule polymer status is also known to be related to adaptive responses. For example, many environmental triggers, such as cold and osmotic stress, are associated with the reorganization of the cytoskeleton (Blancaflor and Hasenstein, 1995; Sangwan et al., 2001; Wojtaszek et al., 2007). The recent discovery that a receptor-like kinase may act as a cell wall integrity sensor suggests that internal as well as external stresses could be an aspect of the adaptive response (Hématy et al., 2007). It is possible, therefore, that detection of a change in cell wall status caused by loss of the *CSLD2* and *CSLD3* product affects cytoskeletal organization, which could in turn also affect cellulose microfibril deposition and amplify the phenotypic effect. Alternatively, given that cytoskeletal reorganization was mostly associated with bulges and previously ruptured root hairs, the remodeling of the cytoskeleton we observed here could be an indirect result of these morphological disturbances rather than direct sensing of changes in cell wall integrity. However, it was shown recently that general disturbances to cell wall structure that lead to morphological changes in the cell do not always lead to altered cortical microtubule organization. Thus, the genetic disruption of cell wall properties may be more strongly correlated to cytoskeletal organization than to cell morphology per se (Paredez et al., 2008).

MATERIALS AND METHODS

Plant Material and Growth Conditions

Arabidopsis (*Arabidopsis thaliana*) T-DNA knockout lines *csld1-1* (SALK_043260), *csld2-1* (SALK_119808), *csld3-1* (CS899; Wang et al., 2001), *csld3-2* (SALK_112105), and *csld4-1* (SAIL_13_H04) were obtained from the Nottingham Arabidopsis Stock Centre. *csld2-2* was obtained from a forward genetic screen for mutants with abnormal root hairs. All of the insertional mutants were in the Col-0 background, except for *csld3-1*, which was in the Wassilewskija background (Wang et al., 2001), and *csld4-1*, which was in the *qrt* background. The correct insertion sites were confirmed by PCR using oligonucleotides specific for each insertion line. All work presented here for *CSLD2* and *CSLD3* was carried out in homozygous lines, and the homozygosity was confirmed in two successive generations. *csld1-1* and *csld4-1* were confirmed to be heterozygous using PCR and PCR plus BASTA selection,

respectively. Seeds were surface sterilized, sown on plates containing Murashige and Skoog medium (1× Murashige and Skoog salts, 8 g L^{-1} agar, 1× B5 vitamins, and 10.8 g L^{-1} Suc), and incubated for 48 h at 4°C in the dark. For root growth and root hair microscopy, plates were incubated vertically for 5 d at 21°C with a 16-h photoperiod. For all other purposes, plates were incubated horizontally for 1 week and seedlings were transferred to soil at 19°C with a 16-h photoperiod. For time-lapse microscopy and DIC experiments, seeds were germinated directly on 0.5% phyta-agar supplemented with 0.5× Murashige and Skoog salts layered onto 62- × 48-mm sterile glass coverslips as described previously (Blancaflor et al., 2003). For complementation experiments, 7-week-old *csld2-1* and *csld4-1* plants were vacuum infiltrated with suspensions of the *Agrobacterium tumefaciens* strain GV3101 bearing constructs containing the corresponding genomic fragment, including the promoter region, using previously described procedures (Bernal et al., 2007).

Semiquantitative RT-PCR Analysis

Total RNA was extracted from roots, leaves, stems, and flowers of wild-type Arabidopsis plants using the RNeasy Plant Mini Kit (Qiagen). For removal of contaminating genomic DNA, RNA samples were incubated in RNase-free DNaseI (Invitrogen). RT-PCR was carried out using 500 ng of total RNA with the Omniscript RT kit (Qiagen) following the manufacturer's protocol. Primers used for *CSLD1* were CSDL1-RT-F (5′-CAATTCT-CACCTTTGAAGCTATG-3′) and CSLD1-RT-R (5′-GGCACTTTGCTCAT-GATCTG-3′) to generate a 445-bp product; primers used for *CSLD4* were CSLD4-RT-F (5′-ACGTGATGCCATGTGAATGC-3′) and CSLD4-RT-R (5′-CTTCATCCATATCATCGC-3′) to generate a 327-bp product; primers used for *CSLD2* were CSLD2-RT-f (5′-GATGGAGATGGTGACGGTATG-3′) and CSLD2-RT-r (5′-AGCTCACAAACCACAGACATTC-3′) to generate a 221-bp product; primers used for *CSLD3* were CSLD3-RT-f (5′-AGTCTGGTTTGAT-GAGGAGTC-3′) and CSLD3-RT-r (5′-ACAACAATTCGGATAAGTATC-3′) to generate a 255-bp product. Arabidopsis translation initiation factor EIF4A2 forward (5′-GAATCTTCTTAGGGGTATCTATGC-3′) and reverse (5′-CTA-TGACATATTCCAGCTTCTCCC-3′) primers were used as a control.

Histochemical Staining for GUS Activity

Histochemical staining of whole plant seedlings for GUS activity was performed as described by Jefferson et al. (1987). Briefly, seedlings growing under agar medium were soaked in GUS substrate solution of 100 mM sodium phosphate, pH 7.0, 0.2% (v/v) Triton X-100, 2.5 mM potassium ferricyanide, 2.5 mM potassium ferrocyanide, and 2 mM 5-bromo-4-chloro-3-indolyl-β-D-glucuronide and then incubated at room temperature for 24 h. Samples were then washed with 100 mM sodium phosphate, pH 7.0, three to five times to remove the background stain. GUS-positive samples were examined with a Nikon Microphot-FX compound microscope equipped with DIC optics, and images of roots were captured using a Nikon DXM 1200 camera.

Pollen Microscopy

For staining of pollen grains with toluidine blue, anthers were collected from 8-week-old plants and fixed, dehydrated, and resin embedded as described by Orfila et al. (2001). Sections were stained with toluidine blue as described previously (Manfield et al., 2004; Bernal et al., 2007) and observed using a light microscope (BH2; Olympus; http://www.olympusglobal.com), and images were collected using a 36-bit digital camera (Coolsnap; Media Cybernetics; http://www.mediacy.com).

Time-Lapse Microscopy of Living Root Hairs

Coverslips containing 3- to 4-d-old seedlings were transferred directly onto the stage of an inverted Nikon TE300 compound microscope equipped with DIC optics. Images of growing root hairs were captured every 1 min over a 2-h time period using a Hamamatsu C2400-75i camera running on Metamorph 6.3 image-acquisition software (Molecular Devices).

Transmission Electron Microscopy

Three-day-old wild-type and *csld2-1* and *csld3-2* seedlings were fixed in 2.5% glutaraldehyde and postfixed in 1% OsO_4 for 2 h at room temperature. Roots were dehydrated through a graded ethanol series and embedded in Spurr's epoxy resin (Electron Microscopy Science). Root hair longitudinal (oblique to the main root axis) sections were cut with an Ultracut E microtome (Reichert-Jung). Ultrathin sections (90–100 nm) were mounted onto 200-mesh copper grids and stained with 1% aqueous uranyl acetate and Reynolds lead citrate solution. The sections were examined and photographed at 80 kV with a Philips CM12 transmission electron microscope. All of the photographs were converted to digital images with a ScanMaker 8700 scanner (Microtek).

In Vitro Pollen Germination and Transmission Assays

Pollen germination assays were carried out using the procedures described by Boavida and McCormick (2007) with slight modifications. Anthers were extracted from flowers of 7- to 10-week-old plants using fine forceps. Pollen grains were evenly spread over a microscope slide containing pollen germination medium (Taylor et al., 1998) using a dissecting microscope. Slides were placed in a tip box with approximately 30 mL of water in the bottom and incubated at 25°C under constant light for 6 to 7 h. Pollen germination efficiency was assessed by counting germinated grains using a light microscope (BH2; Olympus). Images were collected using a digital camera. For the transmission analyses, all crosses were performed by emasculating flowers from 7- to 10-week-old plants and fertilizing with pollen from 7- to 13-week-old plants at 1 d after the emasculation. Seeds were allowed to set; they were carefully collected and grown directly in soil at 19°C with a 16-h photoperiod. BASTA was applied to seedlings from the crosses at 3 and 4 weeks after germination at a concentration of 250 mg L^{-1}.

Cloning Procedures

All complementation experiments were carried out by transformation of the genomic fragments of *CSLD2* and *CSLD4*, including the putative promoter region. The *CSLD2* clone was generated in two steps. One fragment was amplified from bacterial artificial chromosome F20K13 (Arabidopsis Biological Resource Center) using oligonucleotides that annealed 1,950 bp upstream from the *CSLD2* start codon (5′-GAGTTTTGGTTCGGGAATGA-3′) and 1,185 bp downstream of the stop codon (5′-TCACGTACCTGCACCCATAA-3′). This product was digested with *Eco*RI and *Bam*HI, and the resulting fragment was cloned in the corresponding sites in pCAMBIA3300. The second fragment was amplified using oligonucleotides that annealed 1,950 bp upstream of the *CSLD2* start codon (5′-GAGTTTTGGTTCGGGAATGA-3′) and 2,049 bp inside the predicted *CSLD2* open reading frame (5′-*Hin*dIII-TCGCAGAAGCTCT-GACTAAGG-3′). This was cloned into pGEM Teasy (Promega). The *Hin*dIII fragment from this clone was subcloned into the *Hin*dIII site from the plasmid generated in the first step. The orientation of the resulting clone was verified by restriction digestion and sequencing.

The *CSLD4* clone for complementation was generated by amplification from the bacterial artificial chromosome F20D10 using oligonucleotides that annealed 1,573 bp upstream of the predicted *CSLD4* start codon (5′-*Sal*I-ACGCTGCGTTTCTTTCATT-3′) and 402 bp downstream of the stop codon (5′-*Sal*I-CACGGAGGAGGAAGACAGAC-3′). The resulting fragment was cloned into pGEM Teasy and subcloned into the *Sal*I site of pCAMBIA2300.

For subcellular localizations, recombinant proteins with fluorescent tags were constructed as follows. The genomic region of *AtCSLD2* was amplified with primers 5′-ATGGCATCTAATAAGCATTTTG-3′ and 5′-TCATGGAA-AACTGAAGTTTCC-3′. The genomic region of *CSLD4* was amplified with primers 5′-ATGGCGTCCACGCCT-3′ and 5′-TTACGGGAATTGAAAAC-CAC-3′. The amplicons were obtained from genomic Arabidopsis DNA using Phusion polymerase (Finnzymes). The resulting PCR products were purified by the QIAquick PCR Purification Kit (Qiagen) and subsequently functioned as templates in the following USER clonings (Nour-Eldin et al., 2006). YFP-CSLD2 and YFP-CSLD4 were obtained by USER cloning of *CSLD2* and *CSLD4* into the unique USER site in pCAMBIA330035SuYFP in-frame with the downstream YFP (Bernal et al., 2007). In the case of *CSLD2*, primers 5′-GGCTTAAUATGGCATCTAATAAGCATTTTG-3′ and 5′-GGTTTAAUTC-ATGGAAAACTGAAGTTTCC-3′ were used, and in the case of *AtCSLD4*, primers 5′-GGCTTAAUATGGCGTCCACGCCT-3′ and 5′-GGTTTAAUTTAC-GGGAATTGAAAACCAC-3′ were used. Underlined oligonucleotides were engineered to provide USER cloning sites and in such a way that the reading frames of *CSLD2* and *CSLD4* were in frame with the upstream YFP of the N-terminal fusion vector (Nour-Eldin et al., 2006). The cloned PCR products and vector-insert junctions were subsequently verified by sequencing.

For the expression studies, the promoters of *CSLD2* and *CSLD3* were PCR amplified from genomic DNA using the primers 5′-AGTTAGGATC-

TAACTTGGC-3′ and 5′-ATCTGAAAACCTGAGACTGAG-3′ (*CSLD2*) and 5′-TGTCTAATAATAACACTATCCAC-3′ and 5′-GGTGGGAATACAAACC-ATG-3′ (*CSLD3*) using Phusion polymerase (Finnzymes). The resulting PCR products were subsequently cloned in pBGF-0 (Chytilova et al., 1999) using the USER method (Nour-Eldin et al., 2006) and the primers 5′-GGT-TTAAUAGTTAGGATCTAACTTGGC-3′ and 5′-GGCTTAAUATCTGAAA-ACCTGAGACTGAG-3′ (*CSLD2*) and 5′-GGTTTAAUTGTCTAATAATAA-CACTATCCAC-3′ and 5′-GGCTTAAUGGTGGGAATACAAACCATG-3′ (*CSLD3*), resulting in pro*CSLD2*::GFP::GUS and pro*CSLD3*::GFP::GUS, respectively. Inserts and insert-vector junctions were subsequently verified by sequencing.

Plant Transformation

For complementation experiments, flowers from 7-week-old *csld2-1* and *csld4-1* plants were vacuum infiltrated with suspensions of the *A. tumefaciens* strain GV3101 bearing constructs containing the corresponding genomic fragment, including the promoter region, using previously described procedures (Clough and Bent, 1998). *csld2-1* plants were transformed with pCAMBIA3300 bearing the genomic fragment of *CSLD2*. Transformants were selected for BASTA resistance and verified by PCR. *csld4-1* plants were transformed with pCAMBIA2300 bearing the genomic fragment of *CSLD4*. Transformants were selected for kanamycin resistance and verified by PCR. Transformations for promoter studies were carried out in a similar manner, except that the plasmid pBGF-0 and the *A. tumefaciens* strain C58C1 pGV3850 were employed.

Subcellular Localization of CSLD2 and CSLD4

The vectors containing YFP-CSLD2 and YFP-CSLD4 were transformed into *A. tumefaciens* C58C1 pGV3850. The resulting strains were grown overnight in Luria-Bertani medium, harvested by centrifugation, resuspended in a buffer containing 10 mM MES, 10 mM $MgCl_2$, and 100 μM acetosyringone (optical density at 600 nm = 0.05), and allowed to stand at room temperature for 2 to 3 h. Strains carrying the CSLD2 and CSLD4 fusions were mixed with a strain harboring the 35S:p19 construct for suppression of gene silencing (Voinnet et al., 2003) and with the Golgi marker STtmd-GFP (Boevink et al., 1998) or the endoplasmic reticulum marker GFP-HDEL (Boevink et al., 1996), where indicated. The bacterial mix was infiltrated into leaves of 2- to 4-week-old *Nicotiana benthamiana* plants. For comparison, similar experiments were done in parallel using YFP-CSLD3, which has been characterized previously (Bernal et al., 2007). Infiltrated leaves were observed at 24 to 36 h after infiltration by confocal laser-scanning microscopy (TCS SP2; Leica Microsystems). The GFP and YFP fluorescent signals were monitored by sequential line scanning (switching between detection of GFP and YFP signal) with eight line scans per line. The excitation and detection wavelengths for GFP and YFP were 488 and 514 nm for excitation, and 495 to 510 nm and 565 to 593 nm for detection, respectively.

Imaging Cytoskeletal Organization in Living Root Hairs

csld2-1 and *csld3-2* mutants were crossed with wild-type Arabidopsis plants expressing GFP that binds to microtubules and F-actin. For microtubule labeling, mutants were crossed with plants expressing GFP fused to the microtubule-binding domain (MBD) of the MICROTUBULE-ASSOCIATED PROTEIN4 (Marc et al., 1998). For F-actin labeling, mutants were crossed with plants expressing GFP fused to both the N and C termini of the ACTIN-BINDING DOMAIN2 (ABD2) of Arabidopsis FIMBRIN1 (GFP-ABD2-GFP; Wang et al., 2008). Root hairs of 3-d-old seedlings expressing the fusion proteins were imaged using a Leica TCS SP2 AOBS confocal laser-scanning microscope. GFP was excited using the 488-nm line of the argon laser, and emission was detected at 510 nm.

Supplemental Data

The following materials are available in the online version of this article.

Supplemental Figure S1. In silico expression profiling of the *CSLD* family.

Supplemental Figure S2. RT-PCR analysis of the *CSLD* family.

Supplemental Figure S3. Analysis of promoter activity for *CSLD2* and *CSLD3*.

Supplemental Figure S4. Generation of *CSLD* knockout lines.

Supplemental Figure S5. Functional complementation of *csld3-2* with YFP-CSLD3.

Supplemental Movie S1. Time-lapse microscopy of living *csld2-1* root hairs.

Supplemental Movie S2. Time-lapse microscopy of living *csld2-1* root hairs.

Supplemental Movie S3. Time-lapse microscopy of living *csld2-1* root hairs.

Supplemental Movie S4. Time-lapse microscopy of living *csld3-2* root hairs.

Supplemental Movie S5. Time-lapse microscopy of living *csld3-2* root hairs.

ACKNOWLEDGMENTS

We thank Paul Dupree for insightful comments. Dr. Chris Hawes is thanked for the clones for STtmd-GFP and GFP-HDEL. Thanks to Sonia Gutierrez and Nadia Morales for help with growing plants and PCRs.

Received April 25, 2008; accepted August 29, 2008; published September 3, 2008.

LITERATURE CITED

Bacic A, Harris PJ, Stone BA (1988) Structure and function of plant cell walls. *In* J Preiss, ed, The Biochemistry of Plants, Vol 14. Academic Press, New York, pp 297–371

Baumberger N, Ringli C, Keller B (2001) The chimeric leucine-rich repeat/extensin cell wall protein LRX1 is required for root hair morphogenesis in Arabidopsis thaliana. Genes Dev **15:** 1128–1139

Bernal AJ, Jensen JK, Harholt J, Sørensen S, Moller I, Blaukopf C, Johansen B, de Lotto R, Pauly M, Schelle HV, et al (2007) Disruption of ATCSLD5 results in reduced growth, reduced xylan and homogalacturonan synthase activity and altered xylan occurrence in Arabidopsis. Plant J **52:** 791–802

Blancaflor EB, Hasenstein KH (1995) Growth and microtubule orientation of *Zea mays* roots subjected to osmotic stress. Int J Plant Sci **156:** 774–783

Blancaflor EB, Hou G, Chapman KD (2003) Elevated levels of N-lauroethanolamine, an endogenous constituent of desiccated seeds, disrupt normal root development in Arabidopsis thaliana seedlings. Planta **217:** 206–217

Boavida LC, McCormick S (2007) Temperature as a determinant factor for increased and reproducible in vitro pollen germination in Arabidopsis thaliana. Plant J **52:** 570–582

Boevink P, Oparka K, Santa Cruz S, Martin B, Betteridge A, Hawes C (1998) Stacks on tracks: the plant Golgi apparatus traffics on an actin/ER network. Plant J **15:** 441–447

Boevink P, Santa Cruz S, Hawes C, Harris N, Oparka KJ (1996) Virus-mediated delivery of the green fluorescent protein to the endoplasmic reticulum of plant cells. Plant J **10:** 935–941

Böhme K, Li Y, Charlot F, Grierson C, Marrocco K, Okada K, Laloue M, Nogué F (2004) The Arabidopsis COW1 gene encodes a phosphatidylinositol transfer protein essential for root hair tip growth. Plant J **40:** 686–698

Buckeridge MS, Rayon C, Urbanowicz B, Tine MAS, Carpita NC (2004) Mixed linkage (1-3),(1-4)-β-D-glucans of grasses. Cereal Chem **81:** 115–127

Burk DH, Ye ZH (2002) Alteration of oriented deposition of cellulose microfibrils by mutation of a katanin-like microtubule-severing protein. Plant Cell **14:** 1–17

Burton RA, Jobling SA, Harvey AJ, Shirley NJ, Mather DE, Bacic A, Fincher GB (2008) The genetics and transcriptional profiles of the cellulose synthase-like HvCslF gene family in barley. Plant Physiol **146:** 1821–1833

Burton RA, Wilson SM, Hrmova M, Harvey AJ, Shirley NJ, Medhurst A, Stone BA, Newbigin EJ, Bacic A, Fincher GB (2006) Cellulose synthase-

like CslF genes mediate the synthesis of cell wall (1,3;1,4)-β-D-glucans. Science **311:** 1940–1942

Carol RJ, Dolan L (2002) Building a hair: tip growth in Arabidopsis thaliana root hairs. Philos Trans R Soc Lond B Biol Sci **357:** 815–821

Carpita NC, Gibeaut DM (1993) Structural models of primary cell walls in flowering plants: consistency of molecular structure with the physical properties of the walls during growth. Plant J **3:** 1–30

Cavalier DM, Lerouxel O, Neumetzler L, Yamauchi K, Reinecke A, Freshour G, Zabotina OA, Hahn MG, Burgert I, Pauly M, et al (2008) Disrupting two *Arabidopsis thaliana* xylosyltransferase genes results in plants deficient in xyloglucan, a major primary cell wall component. Plant Cell **20:** 1519–1537

Chu Z, Chen H, Zhang Y, Zhang Z, Zheng N, Yin B, Yan H, Zhu L, Zhao X, Yuan M, et al (2007) Knockout of the AtCESA2 gene affects microtubule orientation and causes abnormal cell expansion in Arabidopsis. Plant Physiol **143:** 213–224

Chytilova E, Macas J, Galbraith DW (1999) Green fluorescent protein targeted to the nucleus, a transgenic phenotype useful for studies in plant biology. Ann Bot (Lond) **83:** 645–654

Clough SJ, Bent AF (1998) Floral dip: a simplified method for Agrobacterium-mediated transformation of Arabidopsis thaliana. Plant J **16:** 735–743

Cocuron JC, Lerouxel O, Drakakaki G, Alonso AP, Liepman AH, Keegstra K, Raikhel N, Wilkerson CG (2007) A gene from the cellulose synthase-like C family encodes a beta-1,4 glucan synthase. Proc Natl Acad Sci USA **104:** 8550–8555

Cole RA, Fowler JE (2006) Polarized growth: maintaining focus on the tip. Curr Opin Plant Biol **9:** 579–588

Cosgrove D (2005) Growth of the plant cell wall. Nat Rev Mol Cell Biol **6:** 850–861

Desprez T, Juraniec M, Crowell EF, Jouy H, Pochylova Z, Parcy F, Höfte H, Gonneau M, Vernhettes S (2007) Organization of cellulose synthase complexes involved in primary cell wall synthesis in Arabidopsis thaliana. Proc Natl Acad Sci USA **104:** 15572–15577

Dhugga KS, Barreiro R, Whitten B, Stecca K, Hazebroek J, Randhawa GS, Dolan M, Kinney AJ, Tomes D, Nichols S, et al (2004) Guar seed beta-mannan synthase is a member of the cellulose synthase super gene family. Science **303:** 363–366

Doblin MS, De Melis L, Newbigin E, Bacic A, Read SM (2001) Pollen tubes of *Nicotiana alata* express two genes from different beta-glucan synthase families. Plant Physiol **125:** 2040–2052

Dunkley TP, Hester S, Shadforth IP, Runions J, Weimar T, Hanton SL, Griffin JL, Bessant C, Brandizzi F, Hawes C, et al (2006) Mapping the Arabidopsis organelle proteome. Proc Natl Acad Sci USA **103:** 6518–6523

Emons AMC, Hofte H, Mulder BM (2007) Microtubules and cellulose microfibrils: How intimate is their relationship? Trends Plant Sci **12:** 279–281

Favery B, Ryan E, Foreman F, Linstead P, Boudonck K, Steer M, Shaw P, Dolan L (2001) KOJAK encodes a cellulose synthase-like protein required for root hair cell morphogenesis in Arabidopsis. Genes Dev **15:** 79–89

Fry SC (2004) Primary cell wall metabolism: tracking the careers of wall polymers in living plant cells. New Phytol **161:** 641–675

Goubet F, Misrahi A, Park SK, Zhang Z, Twell D, Dupree P (2003) AtCSLA7, a cellulose synthase-like putative glycosyltransferase, is important for pollen tube growth and embryogenesis in Arabidopsis. Plant Physiol **131:** 547–557

Grierson CS, Roberts K, Feldmann KA, Dolan L (1997) The COW1 locus of Arabidopsis acts after RHD2, and in parallel with RHD3 and TIP1, to determine the shape, rate of elongation, and number of root hairs produced from each site of hair formation. Plant Physiol **115:** 981–990

Gunawardena AH, Greenwood JS, Dengler NG (2004) Programmed cell death remodels lace plant leaf shape during development. Plant Cell **16:** 60–73

Hématy K, Sado PE, Van Tuinen A, Rochange S, Desnos T, Balzergue S, Pelletier S, Renou JP, Höfte H (2007) A receptor-like kinase mediates the response of Arabidopsis cells to the inhibition of cellulose synthesis. Curr Biol **17:** R541–R542

Himmel ME, Ding SY, Johnson DK, Adney WS, Nimlos MR, Brady JW, Foust TD (2007) Biomass recalcitrance: engineering plants and enzymes for biofuels production. Science **315:** 804–807

Honys D, Twell D (2004) Transcriptome analysis of haploid male gametophyte development in Arabidopsis. Genome Biol **5:** R85

Jefferson RA, Kavanagh TA, Bevan MW (1987) GUS fusion: beta-glucuronidase as a sensitive and versatile gene fusion marker in higher plants. EMBO J **6:** 3901–3907

Keegstra K, Walton J (2006) Beta-glucans: brewer's bane, dietician's delight. Science **311:** 1872–1873

Kim CM, Park SH, Je BI, Park SH, Park SJ, Piao HL, Eun MY, Dolan L, Han CD (2007) OsCSLD1, a cellulose synthase-like D1 gene, is required for root hair morphogenesis in rice. Plant Physiol **143:** 1220–1230

Kim HJ, Triplett BA (2001) Cotton fiber growth in planta and in vitro: models for plant cell elongation and cell wall biogenesis. Plant Physiol **127:** 1361–1366

Liepman AH, Wilkerson CG, Keegstra K (2005) Expression of cellulose synthase-like (Csl) genes in insect cells reveals that CslA family members encode mannan synthases. Proc Natl Acad Sci USA **102:** 2221–2226

Manfield IW, Orfila C, McCartney L, Harholt J, Bernal AJ, Scheller HV, Gilmartin PM, Mikkelsen JD, Knox JP, Willats WG (2004) Novel cell wall architecture of isoxaben-habituated Arabidopsis suspension-cultured cells: global transcript profiling and cellular analysis. Plant J **40:** 260–275

Marc J, Granger CL, Brincat J, Fisher DD, Kao TH, McCubbin AG, Cyr RJ (1998) A GFP-MAP4 reporter gene for visualizing cortical microtubule rearrangements in living epidermal cells. Plant Cell **10:** 1927–1940

Mellerowicz EJ, Baucher M, Sundberg B, Boerjan W (2001) Unravelling cell wall formation in the woody dicot stem. Plant Mol Biol **47:** 239–274

Nour-Eldin HH, Hansen BG, Norholm MHH, Jensen JK, Halkier BA (2006) Advancing uracil-excision based cloning towards an ideal technique for cloning PCR fragments. Nucleic Acids Res **34:** e122

O'Neill M, Albersheim P, Darvill A (1990)The pectic polysaccharides of primary cell walls. *In* PM Dey, ed, Methods in Plant Biochemistry, Vol 2. Academic Press, London, pp 415–441

Orfila C, Seymour GB, Willats WG, Huxham IM, Jarvis MC, Dover CJ, Thompson AJ, Knox JP (2001) Altered middle lamella homogalacturonan and disrupted deposition of (1-5)-α-L-arabinan in the pericarp of Cnr, a ripening mutant of tomato. Plant Physiol **126:** 210–221

Paredez AR, Persson S, Ehrhardt DW, Somerville CR (2008) Genetic evidence that cellulose synthase activity influences microtubule cortical arrays activity. Plant Physiol **147:** 1723–1734

Paredez AR, Somerville CR, Ehrhardt DW (2006) Visualization of cellulose synthase demonstrates functional association with microtubules. Science **312:** 1491–1495

Parton RM, Dyer AF, Read ND, Trewava AJ (2000) Apical structure of actively growing fern rhizoids examined by DIC and confocal microscopy. Ann Bot (Lond) **85:** 233–245

Persson S, Caffall KH, Freshour G, Hilley MT, Bauer S, Poindexter P, Hahn MG, Mohnen D, Somerville C (2007) The *Arabidopsis irregular xylem8* mutant is deficient in glucuronoxylan and homogalacturonan, which are essential for secondary cell wall integrity. Plant Cell **19:** 237–255

Reiter WD (2002) Biosynthesis and properties of the plant cell wall. Curr Opin Plant Biol **5:** 536–542

Reyna-Villasmil N, Bermúdez-Pirela V, Mengual-Moreno E, Arias N, Cano-Ponce C, Leal-Gonzalez E, Souki A, Inglett GE, Israili ZH, Hernández-Hernández R, et al (2007) Oat-derived beta-glucan significantly improves HDLC and diminishes LDLC and non-HDL cholesterol in overweight individuals with mild hypercholesterolemia. Am J Ther **14:** 203–212

Rhee SY, Somerville CR (1998) Tetrad pollen formation in quartet mutants of Arabidopsis thaliana is associated with persistence of pectic polysaccharides of the pollen mother cell wall. Plant J **15:** 79–88

Richmond TA, Somerville CR (2000) The cellulose synthase superfamily. Plant Physiol **124:** 495–498

Richmond TA, Somerville CR (2001) Integrative approaches to determining Csl function. Plant Mol Biol **47:** 131–143

Ridley BL, O'Neill MA, Mohnen D (2001) Pectins: structure, biosynthesis, and oligogalacturonide-related signaling. Phytochemistry **57:** 929–967

Roberts AW, Bushoven JT (2007) The cellulose synthase (CESA) gene superfamily of the moss Physcomitrella patens. Plant Mol Biol **63:** 207–219

Samuga A, Joshi CP (2004) Cloning and characterization of cellulose synthase-like gene, PtrCSLD2 from developing xylem of aspen trees. Physiol Plant **120:** 631–641

Sangwan V, Foulds I, Singh J, Dhindsa RS (2001) Cold-induction of Brassica napus gene, BN115, is mediated by structural changes in the membrane and cytoskeleton and requires Ca^{2+} influx. Plant J **27:** 1–2

Scheible WR, Pauly M (2004) Glycosyltransferases and cell wall biosynthesis: novel players and insights. Curr Opin Plant Biol **7:** 285–295

Sørensen I, Pettolino FA, Wilson SM, Doblin MS, Johansen B, Bacic A, Willats WGT (2008) Mixed linkage (1→3),(1→4)-β-D-glucan is not unique to the Poales and is an abundant component of Equisetum arvense cell walls. Plant J **54:** 510–521

Sterling JD, Atmodjo MA, Inwood SE, Kumar Kolli VS, Quigley HF, Hahn MG, Mohnen D (2006) Functional identification of an Arabidopsis pectin biosynthetic homogalacturonan galacturonosyltransferase. Proc Natl Acad Sci USA **103:** 5236–5241

Sugimoto K, Himmelspach R, Williamson RE, Wasteneys GO (2003) Mutation or drug-dependent microtubule disruption causes radial swelling without altering parallel cellulose microfibril deposition in *Arabidopsis* root cells. Plant Cell **15:** 1414–1429

Taylor NG, Howells RM, Huttly AK, Vickers K, Turner SR (2003) Interactions among three distinct CesA proteins essential for cellulose synthesis. Proc Natl Acad Sci USA **100:** 1450–1455

Taylor PE, Glover JA, Lavithis M, Craig S, Singh MB, Knox RB, Dennis ES, Chaudhury AM (1998) Genetic control of male fertility in Arabidopsis thaliana: structural analyses of postmeiotic developmental mutants. Planta **205:** 492–505

Voinnet O, Rivas S, Mestre P, Baulcombe D (2003) An enhanced transient expression system in plants based on suppression of gene silencing by the p19 protein of tomato bushy stunt virus. Plant J **33:** 949–56

Wang X, Cnops G, Vanderhaeghen R, De Block S, Van Montagu M, Van Lijsebettens M (2001) AtCSLD3, a cellulose synthase-like gene important for root hair growth in Arabidopsis. Plant Physiol **126:** 575–586

Wang YS, Yoo CM, Blancaflor EB (2008) Improved imaging of actin filaments in transgenic Arabidopsis plants expressing a green fluorescent protein fusion to the C and N terminus of the fimbrin actin binding domain 2. New Phytol **177:** 525–536

Wasteneys GO (2004) Progress in understanding the role of microtubules in plant cells. Curr Opin Plant Biol **7:** 651–660

Willats WGT, Knox JP, Mikkelsen JD (2006) Pectin: new insights into an old polymer are starting to gel. Trends Food Sci Technol **17:** 97–104

Wojtaszek P, Baluška F, Kasprowicz A, Luczak M, Volkmann D (2007) Mechanosensory transmission of cell wall disturbances to the actin cytoskeleton in maize root apex cells. Protoplasma **230:** 217–230

Zeng W, Keegstra K (2008) AtCSLD2 is an integral Golgi membrane protein with its N-terminus facing the cytosol. Planta **228:** 823–838

Zhu Y, Nam J, Carpita NC, Matthysse AG, Gelvin SB (2003) Agrobacterium-mediated root transformation is inhibited by mutation of an Arabidopsis cellulose synthase-like gene. Plant Physiol **133:** 1000–1010